Experimental Demonstration of Spectrally Efficient Frequency Division Multiplexing Transmissions at E-Band

Hedaia Ghannam, *Student Member, IEEE*, Dhecha Nopchinda, *Student Member, IEEE,* Marcus Gavell, *Graduate Student Member, IEEE,* Herbert Zirath, *Fellow, IEEE,* and Izzat Darwazeh, *Senior Member, IEEE*

***Abstract*— This paper presents the design and the experimental demonstration of transmission of spectrally efficient frequency division multiplexing (SEFDM) signals, using a single 5-GHz channel, from 81 to 86 GHz in the E-band frequency allocation. A purpose-built E-band SEFDM experimental demonstrator, consisting of transmitter and receiver GaAs microwave integrated circuits, along with a complete chain of digital signal processing is explained. Solutions are proposed to solve the channel and phase offset estimation and equalization issues, which arise from the well-known intercarrier interference between the SEFDM signal subcarriers. This paper shows the highest transmission rate of 12 Gb/s over a bandwidth varying between 2.67 to 4 GHz depending on the compression level of the SEFDM signals, which results in a spectral efficiency improvement by up to 50%, compared to the conventional orthogonal frequency division multiplexing modulation format.**

***Index Terms*— E-band, E-band transceiver, intercarrier interference (ICI), millimeter wave, multicarrier, orthogonal frequency division multiplexing (OFDM), spectral efficiency, spectrally efficient frequency division multiplexing (SEFDM).**

I. Introduction

THE continuous growth of data-hungry services pushes the current microwave spectrum toward saturation. Recently, the research interest has shifted to higher frequencies to benefit from the larger available bandwidth (BW). The E-band, defined from 71 to 76 GHz and 81 to 86 GHz, is worthwhile investigating for multiple reasons.

Manuscript received December 13, 2018; accepted February 6, 2019. Date of publication March 21, 2019; date of current version May 6, 2019. This work was supported in part by the Engineering and Physical Sciences Research Council (EPSRC), Impact Acceleration Account (IAA) Award (EP/R511638/1) held in UCL Innovation and Enterprise. The work of H. Ghannam was supported in part by the Overseas Research Student Award and in part by the UCL Dean of Engineering Sciences Award *(Corresponding author: Hedaia Ghannam.)*

H. Ghannam and I. Darwazeh are with the Communication and Information System Group, Department of Electronics and Electrical Engineering, University College London, London WC1E 6BT, U.K. (e-mail: hedaia.ghannam.15@ucl.ac.uk; i.darwazeh@ucl.ac.uk).

D. Nopchinda and H. Zirath are with the Microwave Electronics Laboratory, Department of Microtechnology and Nanoscience, Chalmers University of Technology, 412 96 Gothenburg, Sweden (e-mail: dhecha@chalmers.se; herbert.zirath@chalmers.se).

M. Gavell is with Gotmic AB, 411 33 Gothenburg, Sweden (e-mail: marcus.gavell@gotmic.se).

Color versions of one or more of the figures in this paper are available online at http://ieeexplore.ieee.org.

Digital Object Identifier 10.1109/TMTT.2019.2901667

1) The 5–10 GHz of available bandwidth BW allows multi-gigabits per second transmission.
2) The low atmospheric absorption compared to the 60 GHz and beyond −100 GHz bands allows data transmission over a relatively long distance.
3) The light-licensing requirements of the E-band spectrum simplify and reduce the operating cost [1].

In a multipath environment, the millimeter-wave channel exhibits frequency-selective characteristics. To combat frequency selectivity and to simplify channel equalization, orthogonal frequency division multiplexing (OFDM) converts the frequency selective channel into a parallel collection of orthogonal frequency flat subchannels [2]. This is the reason of the popularity of OFDM for many of today's wireless applications and experiments. A comprehensive and complete study of OFDM versus single carrier millimeter-wave transmission by Rappaport *et al.* [3] concludes that the superior frequency-selectivity mitigation capabilities of OFDM offset the power amplifier nonlinearity benefits of single carrier, at least when robust channel coding is used. For instance, OFDM is chosen for the WiFi 802.11ad and wireless personal area network IEEE 802.15.3c new standards over the millimeter-wave spectrum [4] and the future 5G standards [1]. Much experiments have been demonstrated on different millimeter bands for OFDM ranging from 39 GHz [5], 40 GHz [6], 60 GHz [7], and up to 94 GHz [8] for different applications and scenarios. More experiments can be found in the references therein of the above-mentioned papers.

Only a few trials have been carried out in the E-band transmission to gain a better understanding of the channel propagation characteristics and to prove its viability. Rappaport *et al.* [3] have investigated the deployment of highly directional steerable antennas with beamforming for data transmission over the (71–76 GHz) spectrum, in an indoor scenario [9] and an outdoor scenario [10] in New York City for future 5G communication systems. A demonstration of adaptive OFDM-based transmission over the 70-GHz band has been reported in [4], where different modulation orders to different subcarriers groups are implemented to cope with channel impairments and enhance system total capacity. Other FDM-based systems have been implemented too, such as the 6 Gb/s demonstrator reported in [11], where the 81–86 GHz

BW is divided into subchannels. Each subchannel is filtered with a root-raised-cosine filter to reduce the interference between subcarriers.

Up to this point, the E-band transmission is limited to orthogonal signals transmission, which constricts the system spectral efficiency. Recent research focuses on enhancing the spectral efficiency by either minimizing the out-of-band emission (OOBE) or by exploiting the signal orthogonality. The substantial motivation behind the 5G modulation candidates analyzed in [12] is to reduce the OOBE. This may be achieved by windowing the symbols in time such as in windowed OFDM [12], or by filtering a group of subcarriers; filtered-OFDM [13] and universal filtered multicarrier are two popular methods along this line [12]. More advanced filtering, of each subcarrier, such as filter bank multicarrier and generalized frequency division multiplexing, represent other candidates for 5G [12], [14] but unfortunately, require new complex transceivers.

A marked contribution of improving spectral efficiency using non-orthogonal signaling formats was proposed back in 1975 by Mazo [15], where it can be shown that in a single-carrier scenario, a 25% gain in spectral efficiency can be achieved at the same bit error rate (BER) and energy per bit E_b. In 2003, a nonorthogonal multicarrier signal format named spectrally efficient frequency division multiplexing (SEFDM) [16] was proposed. In SEFDM, the subcarriers are placed closer in frequency (relative to OFDM) to achieve spectral efficiency gains, while compromising the orthogonality and receiver complexity. The multistream faster than the Nyquist technique initially proposed in [17] and detailed in [18] is SEFDM's time domain counterpart and has similar spectral efficiency gains with little error performance loss relative to OFDM. The recent report of [19] derives an expression which shows that nonorthogonal multicarrier signals have the potential to achieve higher capacity limits compared to orthogonal signals.

Improving the spectral efficiency is not the only motivation for using SEFDM signals [37]. There are also noise advantages when BW is reduced, such as the overall reduction of noise power and as was shown recently in [20]; the impact of white phase noise depends on the BW of the signal. Therefore, the impact of white phase noise in SEFDM will be less than that of OFDM for the same transmission rate, while the severity of near carrier phase noise will not be affected [21], [22]. In addition, improving the achievable spectral efficiency without increasing the constellation cardinality can be considerably convenient, since it is well known that low-order constellations are more robust to channel impairments such as time-varying phase noise and nonlinearities.

SEFDM is an ill-conditioned system, and its practicability is hindered by two main obstacles; signal detection and channel estimation and equalization. For signal detection, the inter-carrier interference (ICI) between subcarriers is conceptually similar to that seen in distorted OFDM albeit, with more detrimental effect. To ameliorate the effect of such ICI, for uncoded systems, different techniques have been successfully developed, such as sphere decoder [23], fixed sphere decoder [24], pulse shaping [25], and iterative detector [26]. Furthermore, forward error correction (FEC) has been proposed and tested either on its own [27], or as a part of an interference canceller that operates iteratively over the received SEFDM symbols to cancel the interference and to improve the performance of coded systems [19], [28].

The nonorthogonality nature of SEFDM signals further complicates the channel estimation problem. Estimation of the system phase offset and channel response has been addressed using various methods, either in the time domain [29], [30] or in the frequency domain [31]. Recently, a new robust channel frequency response (CFR) estimation scheme for SEFDM signals was proposed in [31], and it will be experimentally demonstrated in this paper for the first time. In this estimation scheme, the pilot symbol uses the same number of subcarriers and the same frequency spacing of SEFDM signals used to transmit data, while maintaining the orthogonality. As a result, a simple and accurate channel estimation is guaranteed at the expense of slightly increased pilot duration overhead.

Experimental SEFDM test beds with significant spectral efficiency gains have been demonstrated to serve different applications. In [32], 2.25 Gb/s SEFDM signals were transmitted over the 60 GHz frequency band, and a wireless test bed for future cellular networks has been reported in [33]. The 10 Gb/s optical SEFDM signal transmission systems were reported in [19] and [34], and a 24 Gb/s coherent optical transmission over single-mode fiber have been implemented in [35]. A summary of these systems can be found in [36], and the recent SEFDM systems survey paper [37].

This paper, and for the first time, presents an experimental demonstration of SEFDM signal wireless transmission at a rate of 12 Gb/s over the E-band (81–86 GHz) frequency range. The powerful low-density parity-check (LDPC) FEC codes invented by Gallager [38] and adopted in future cellular 5G standards [39], and the CFR estimation scheme of [31] is used in this experimental demonstration. The experiment results show that the use of SEFDM signals enhances the system spectral efficiency by up to 50% compared to OFDM. This demonstration represents an important milestone for SEFDM transmission at the E-band. Unlike the aforementioned experiments, the employment of LDPC codes and the new CFR estimation scheme with no complex transmitter and receiver signal processing, highlights the potential of a real-time implementation.

This paper is organized as follows. Section II describes the SEFDM signals and the processing schemes used to deal with SEFDM impairments arising from ICI; Section III gives a detailed description of the E-band transmitter and receiver integrated circuits' topology and shows some measurements to prove the suitability of the circuits for this experiment; Section IV describes the SEFDM transmission experimental demonstrator; in Section V, an analysis of the experiment results and measurements are given, and finally, conclusions are drawn in Section VI.

II. SEFDM Waveform

SEFDM is a multicarrier multiplexing technique, where symbols are generated similar to OFDM. For an SEFDM

symbol $x(t)$ with N subcarriers, if $\mathbf{z} = \{z_0, z_1, \ldots, z_{N-1}\}$ are the complex baseband symbols [e.g., QPSK, 8-phase-shift keying (PSK)] of symbol duration T_s and symbol rate $R_s = 1/T_s$, to be modulated by the SEFDM subcarriers, then the complex envelope of the baseband SEFDM-modulated signal is

$$x(t) = \frac{1}{\sqrt{T}} \sum_{n=0}^{N-1} z_n \exp\left(j2\pi\alpha\left(n\Delta f - \frac{R_s}{2}\right)t\right), \quad 0 \le t \le T \tag{1}$$

where $T = N \times T_s$ is the SEFDM symbol duration, while Δf is the frequency spacing between subcarriers. In contrast to OFDM where $\Delta f \times T = 1$, the SEFDM subcarriers are not orthogonal and $\Delta f \times T = \alpha$, given $0 < \alpha < 1$, is the BW compression factor. In this experimental work, α takes two values $4/5$ and $2/3$ to demonstrate a spectral efficiency gain of 25% and 50%, respectively, as will be shown later.

The RF power spectra of OFDM and SEFDM signals at the transmitter are shown in Fig. 1, where the center frequency $f_c = 83.5$ GHz, $N = 16$ subcarriers modulated by QPSK symbols ($M = 4$), $\Delta f = \alpha \times 250$ MHz, $R_s = 4$ Gsymbol/s, and the total BW is BW $= \alpha \times R_s = \alpha \times 4$ GHz. Clearly, SEFDM saves $(1-\alpha)\times 100\%$ BW in comparison to OFDM for the same transmission bit rate, $R_b = \log_2(M) \times R_s = 8$ Gb/s.

The convolution of the transmitter (Tx), the receiver (Rx), and the channel impulse responses may be represented by a frequency-selective multipath vector of L paths. Thus, the received signal can be expressed as

$$y(t) = \sum_{l=1}^{L} \gamma_l x(t - \tau_l) + w(t) \tag{2}$$

where γ_l and τ_l are the complex amplitude and the delay of the l^{th} path, respectively. $w(t)$ is the additive white Gaussian noise (AWGN), with zero mean and variance $\sigma_n^2 = N_0/2$, where N_0 is the noise power spectral density.

The demodulated symbol $\hat{z}_n$, at the n^{th} subcarrier, affected by the channel and contaminated by interference resulting from ICI can be expressed as [31]

$$\begin{aligned}\hat{z}_n &= \frac{1}{\sqrt{T}} \int_0^T y(t) \exp\left(-j2\pi\alpha\left(n\Delta f - \frac{R_s}{2}\right)t\right) dt \\ &= \sum_{m=0}^{N-1} z_m H_m \Lambda(m,n) \\ &\quad + \frac{1}{\sqrt{T}} \int_0^T w(t) \exp\left(-j2\pi\alpha\left(n\Delta f - \frac{R_s}{2}\right)t\right) dt \end{aligned} \tag{3}$$

where $H_m = \sum_L \gamma_l \exp(-j2\pi\alpha(m\Delta f - (R_s/2)\tau_l)$[1] is the multipath CFR acting on the m^{th} subcarrier of the SEFDM symbol, and $\Lambda(m,n)$ is the cross correlation between the subcarriers m and n given by [40]

$$\Lambda(m,n) = \exp(j\pi\alpha(m-n))\text{sinc}(\alpha(m-n)) \tag{4}$$

[1]A subindex m is used instead of n for the transmitted SEFDM signal to distinguish between the transmitted and received.

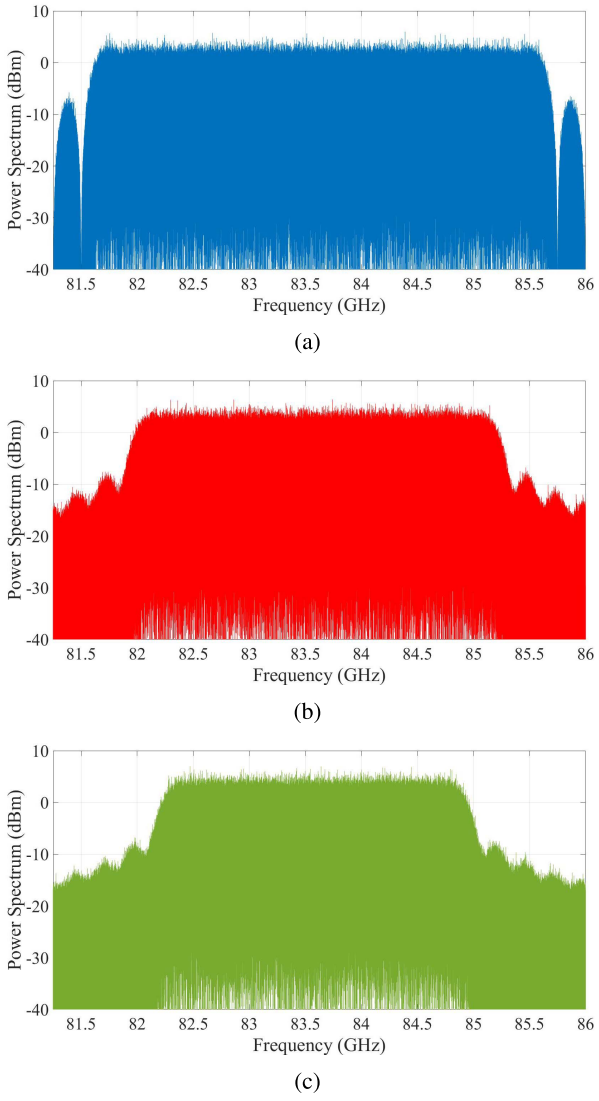

Fig. 1. Comparison of OFDM ($\alpha = 1$) and SEFDM (α = 4/5 and 2/3) spectra at the transmitter for the same transmission rate 8 Gb/s. (a) OFDM ($\alpha = 1$), BW = 4 GHz. (b) SEFDM ($\alpha = 4/5$), BW = 3.2 GHz. (c) SEFDM ($\alpha = 2/3$), BW = 2.67 GHz.

where $\text{sinc}(x) = \sin(\pi x)/\pi x$. The second summation term of (3) on the right-hand side represents the AWGN effect on the n^{th} subcarrier. It is convenient to describe the transmitter and receiver models in the digital domain using a linear model. The digital version is obtained by sampling the signal, at least at the Nyquist rate, to allow the reconstruction of the signal from its samples at the receiver. This implies that $Q \ge N$ samples are required [28]. A demodulated SEFDM symbol $\hat{\mathbf{z}}$ from (3) can be expressed in a matrix form as

$$\hat{\mathbf{z}} = \mathbf{\Lambda H z} + \mathbf{w} \tag{5}$$

where $\hat{\mathbf{z}}$ and $\mathbf{w}$ are $\mathbb{C}^{N\times 1}$ vectors of the demodulated baseband symbol and the white noise, respectively. $\mathbf{H} \in \mathbb{C}^{N\times N}$ is a diagonal matrix, where its diagonal element $H_{n,n}$ is the CFR coefficient of the n^{th} subcarrier of the SEFDM signal and $\mathbf{\Lambda} \in \mathbb{C}^{N\times N}$ is the subcarriers correlation matrix, whose elements are given in (4). Hence, the received signal at the input of

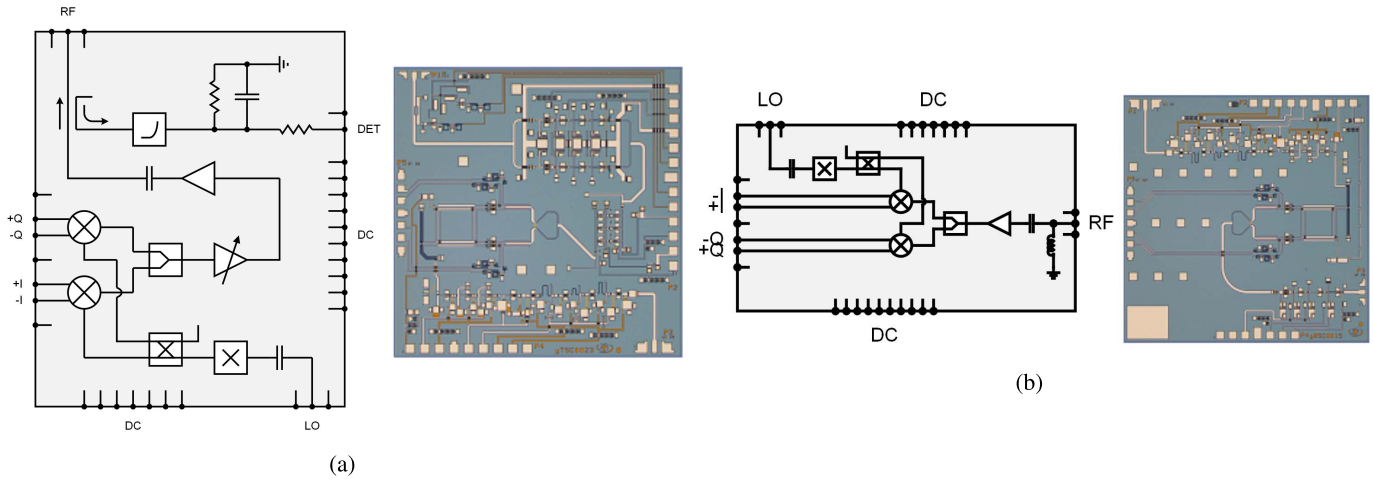

Fig. 2. E-band block diagram [41] and chip photograph. (a) Transmitter, Tx: gTSC0023B. (b) Receiver, Rx: gRSC0014B.

the detector, inside the baseband receiver, suffers from dual distortion; ICI and system impairments.

Direct channel estimation using an SEFDM pilot is impractical due to the ill-conditioned matrix $\mathbf{\Lambda}$ in (5). Recently, a new robust CFR estimation scheme for SEFDM signals was proposed in [31], where the pilot signals are sent over orthogonally spaced subcarriers as an OFDM symbol (i.e., Λ in (5) is an identity matrix). The pilot symbol uses the same number of subcarriers and the same frequency spacing of SEFDM signals used to transmit data. Hence, the frequency allocation of the pilot symbol's OFDM subcarriers is aligned with that of SEFDM. As a result, a simple and accurate channel estimation is guaranteed at the expense of slightly increased pilot duration overhead.

The estimated CFR coefficients are used to equalize the channel and system effects using a simple one-tap equalizer [31]. Consequently, the LDPC decoder, employed for data symbols detection, is capable of dealing with the ICI after equalizing the channel effect, either on its own or as a part of the successive interference canceller introduced in [28].

III. E-Band Transmitter and Receiver Integrated Circuits' Design

The E-band SEFDM monolithic microwave integrated circuit (MMIC) Tx and Rx in the experiment were TSC0023B and RSC0015D, respectively. Both Tx and Rx are designed by Gotmic AB for this collaborative work. Based on WIN Semiconductors' 100 nm GaAs pHEMT process (PP10-10), the Tx and the Rx circuits are one-chip solutions that contain integrated frequency sextupler (X6) and balanced IQ modulator. The two MMICs were each mounted on Taconic Taclamplus printed circuit board (PCB) of size 3×3 mm^2, having 100 μm thick substrate on 1 mm copper hardback with edge-launch SMA connectors for the local oscillator (LO) and IQ ports and a WR12 waveguide interface for the RF. Additional PCBs were used, taking only ± 5 V, for making the E-band SEFDM transmitter and receiver plug"n"play solutions for quick deployment and ease-of-use.

A. Design Topology of the Transmitter and the Receiver

The Tx integrated circuit contains a variable-gain amplifier (VGA), a medium power amplifier, and a power detector for monitoring RF output power and LO leakage. These components are integrated after the quadrature mixer, as shown in the block diagram and the corresponding chip photograph in Fig. 2(a). The quadrature mixer comprises a differential branch line coupler and a Marchand balun on the LO side and is based on the topology in [42]. Such design provides LO-RF isolation and quadrature interface, suitable for direct modulation. The frequency sextupler makes the use of a differential stage amplifier, which in saturation is rich of odd harmonics, and a common-source transistor biased at threshold, which is rich of even harmonics. These two sources extract the X3 and the X2 frequency products respectively, and together with the amplifiers, they boost the signal level, such that the output power level reaches 16 dBm. The detailed schematic of the frequency sextupler is described in [43]. The VGA utilizes a traveling-wave-type amplifier for gain control, which over 25 dB gain control range has consistent flat gain response and return loss better than 10 dB. The medium power amplifier consists of four stages and in two parallel branches to increase linearity. A gradual increase in the gate width of the transistors from 150 to 400 μm has been adopted in the design, to balance the transmitter's power consumption and the third-order intermodulation product. At the output, the RF signal is 10 dB coupled to a power detector; thus, the detector is sensitive enough to detect all the power levels across the gain control range.

In terms of the receiver, the Rx circuit of Fig. 2(b) consists of a low-noise amplifier (LNA) placed in front of the quadrature mixer. The LNA is used to buffer the noise figure, such that the conversion gain and noise figure of the whole receiver chip are 15 and 5 dB, respectively. The LNA consists of a three-stage amplifier design, where the first transistor is biased at a low drain voltage and low current for optimum noise figure. Similar to the medium power amplifier in the transmitter, the second and third stages have a gradual increase in their transistors size to improve linearity. The quadrature mixer and

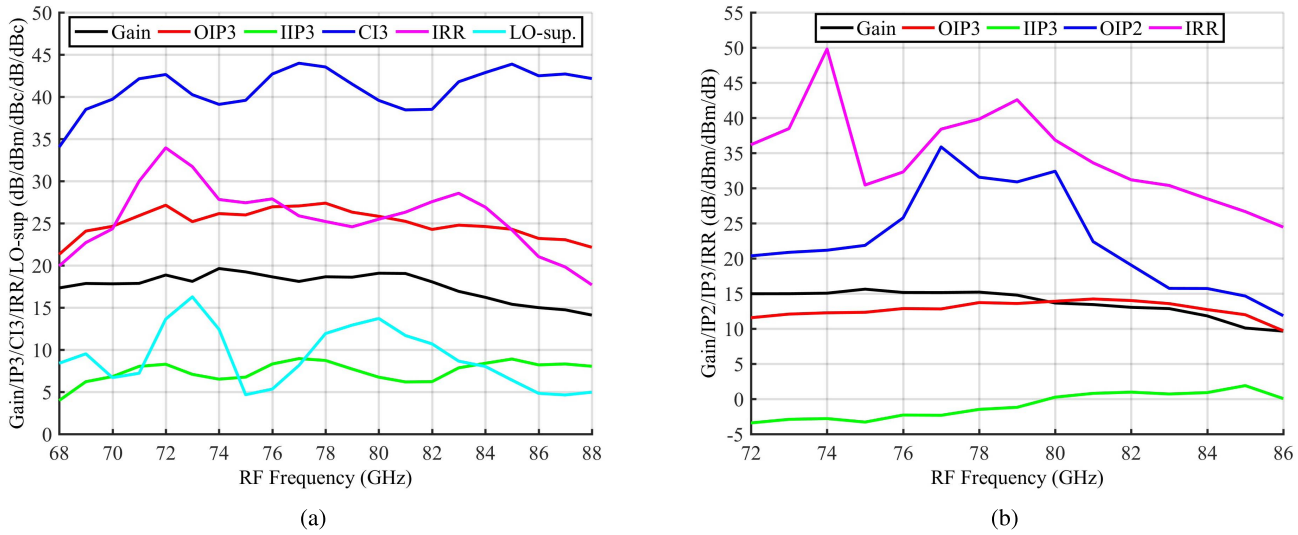

Fig. 3. Measured performance of the SEFDM E-band transmitter and receiver at different RF frequencies. (a) Transmitter. (b) Receiver.

the frequency sextupler are identical to the ones described in the transmitter above.

B. Measurements of the Transmitter and the Receiver

The suitability of the Tx circuit is evaluated in Fig. 3(a). The results show that the measured maximum conversion gain, third-order output intercept point (OIP3), and image rejection ratio (IRR) are 18 dB, 26 dBm, and 25 dB, respectively. This implies that the transmission of multicarrier modulation formats including OFDM and SEFDM even at a relatively high peak-to-average power ratio is viable. Nevertheless, because of the limited frequency response of the branch line coupler, it is noticed that the IRR is high at the center frequency and starts to deviate at the corner frequencies. LO suppression can be further improved (around 40 dBc), by applying dc offset to the $+$I, $-$I and $+$Q, $-$Q channels.

For the receiver, the measured input linearity may be described by measuring the third-order input intercept point (IIP3) and the IRR, which are 1 dBm and 25 dB, respectively, as shown in Fig. 3(b). We can notice that the performance is similar to that of the transmitter, indicating the suitability to multiple-subcarrier modulation format.

For direct modulation and demodulation, intermodulation product, such as IM2, is a critical parameter because it falls within the modulated signal BW. Thus, OIP2 has been measured and the results indicate that OIP2 is higher than 30 dBm at the center frequency, but decreases to 12 dBm at 86 GHz. This effectively limits the maximum received signal power of the SEFDM receiver chain.

IV. E-Band SEFDM Transmission Demonstrator

The experiment was held at the Microwave Electronics Laboratory, Department of Microtechnology and Nanoscience, Chalmers University of Technology, Gothenburg, Sweden. The setup is shown in Fig. 4(a); the Tx chip (TSC0023B) and Rx chip (RSC0015D) are shown in Fig. 4(b) and (c), respectively. The experiment system parameters are summarized in Table I.

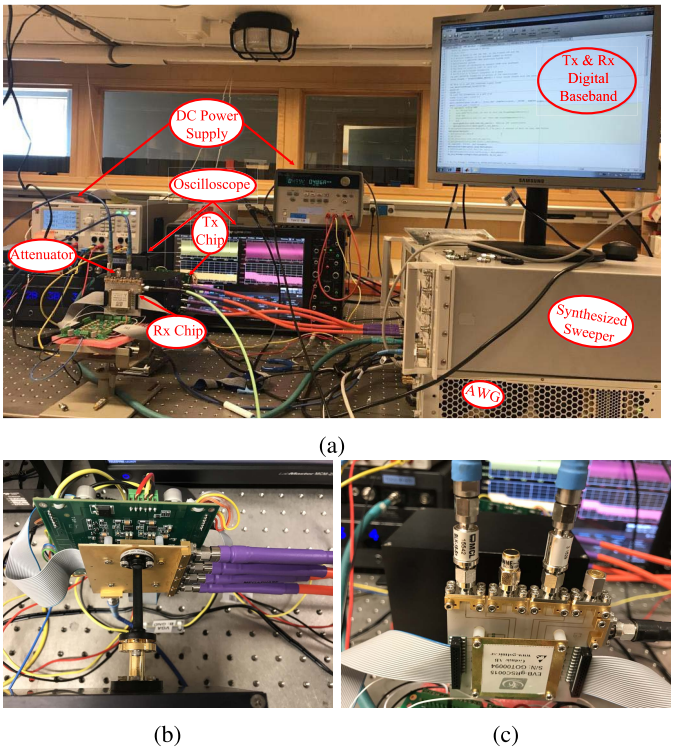

Fig. 4. Photographs of the SEFDM E-band experiment test bed. (a) SEFDM E-band transmission test bed. (b) Transmitter chip. (c) Receiver chip.

A. Experimental Setup

A descriptive block diagram is depicted in Fig. 6, starting from the Tx digital baseband part, to upconversion to radio RF band, to the signal E-band transmission and then downconversion from RF to baseband again to recover the transmitted bits.

The arbitrary waveform generator (AWG) (Keysight M8195A) was used as a digital-to-analog converter, with a vertical resolution of 8 bits, to convert digital baseband signal to analog input to the E-band Tx. The AWG provides two dif-

TABLE I
SYSTEM PARAMETERS

Parameter	Value
Sampling Rate (f_s)	16 Gsample/sec
Number of subcarriers (N)	16
Number of pilot OFDM symbols	5
OFDM/ SEFDM symbol duration (T)	4 ns
Compression factor (α)	$2/3, 4/5, 1$
Pilot symbol duration (T_p)	$4/\alpha$ ns
Subcarrier Bandwidth (Δf)	$\alpha \times 250$ MHz
Bandwidth (BW)	$\alpha \times 4$ GHz
RF Center carrier frequency (f_c)	83.5 GHz
Transmission frequency band	$(-\frac{\alpha \times BW}{2}) - (\frac{\alpha \times BW}{2}) + f_c$
Transmission symbol rate (R_s)	4 Gsymbol/sec
Modulation cardinality (M)	4, 8
LDPC coding rate (R_c)	$1/3$
LDPC decoder number of iteration	50
Interleaver size	64800 bits

ferential outputs (+I, −I, +Q, −Q), each operates at 16 Gsample/s and are connected to the four inputs of the Tx chip (TSC0023B) which upconverts the input signal to the RF range around the center frequency 83.5 GHz. It is important to mention that the AWG buffer size (10 million samples) limits the number of transmitted samples in this experiment. The RF signal propagates through the E-band waveguide (WR12), and the digital variable attenuator (Mi-Wave's 511 Series Precision Programmable Rotary Vane) is inserted to introduce a controlled frequency-selective environment and to avoid the receiver from reaching its saturation region. The measured channel frequency amplitude and phase responses and group delay are shown in Fig. 5. From the measurements, the combination of waveguides and attenuator may be characterized as a frequency-selective channel and almost linear phase resulting in fluctuations in the channel group delay. Such channel appears in a multipath environment, where the signal propagates through different paths.

At the receiver, the Rx chip (RSC0015D) downconverts the RF signal back to the baseband region and the received IQ outputs are connected to the (Teledyne Lab Master 10–100 Zi) oscilloscope, operating as an analog-to-digital converter, with a vertical resolution of 8 bits, at 80 GHz sampling rate (interleaved) and 36 GHz analog BW. The sampled signals are fed to the digital baseband receiver which is implemented offline in MATLAB to recover the transmitted symbols and evaluate system performance as will be discussed in the next section.

B. SEFDM Digital Baseband Tx and Rx

As shown in Fig. 6, at the transmitter, in the first stage, a stream of bits $\mathbf{b} \in \{0, 1\}$ are encoded by the LDPC encoder. The coding rate is defined as the ratio of information bits to the number of coded bits. The coded bits contain the information bits plus parity bits that are generated using the LDPC sparse matrix [44]. Thus, this increases the redundancy of the information bits transmitted, as even if the information bit is lost, still parity check bits can be used to regenerate the information bits at the receiver side. Therefore, by increasing the number of parity bits sent for each information bit, the probability of detecting the transmitted message increases. The drawback of such channel coding is that by sending redundant information, the overall throughput of the system reduces. Channel coding can be looked at as a tradeoff between transmission quality and throughput. In this paper, we use a coding rate ($R_c = 1/3$),

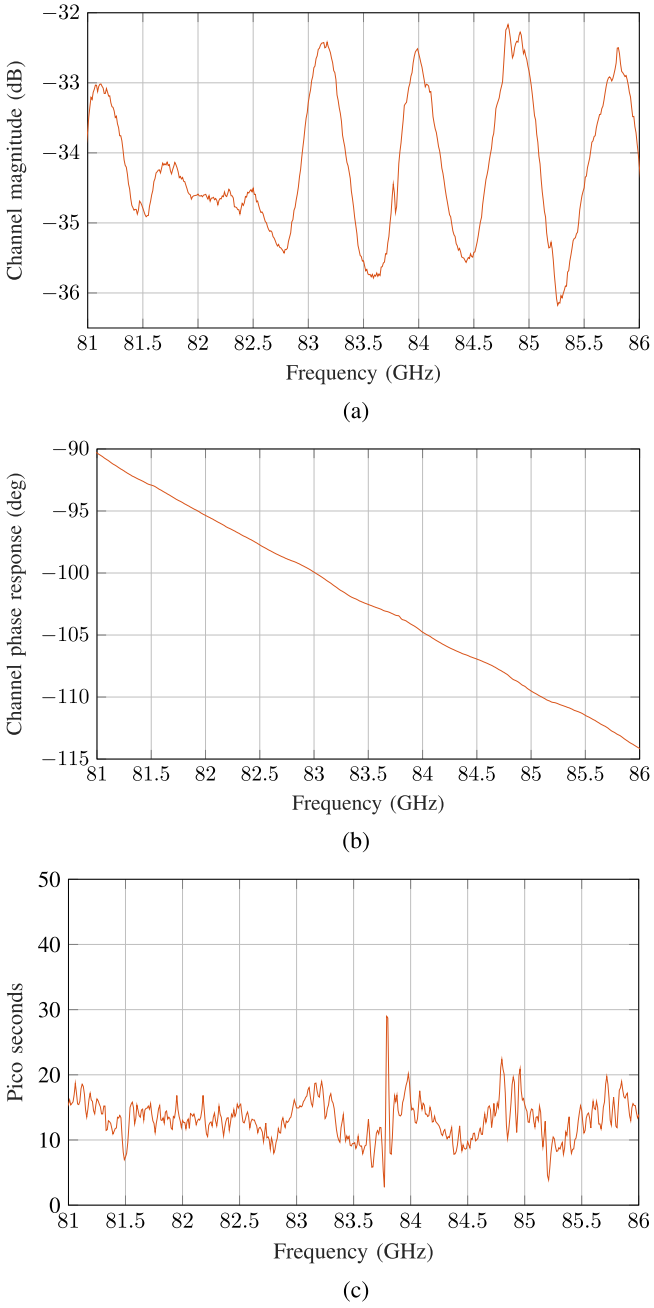

Fig. 5. Attenuator measured channel magnitude, phase response, and group delay. (a) Channel magnitude response. (b) Channel phase response. (c) Channel group delay.

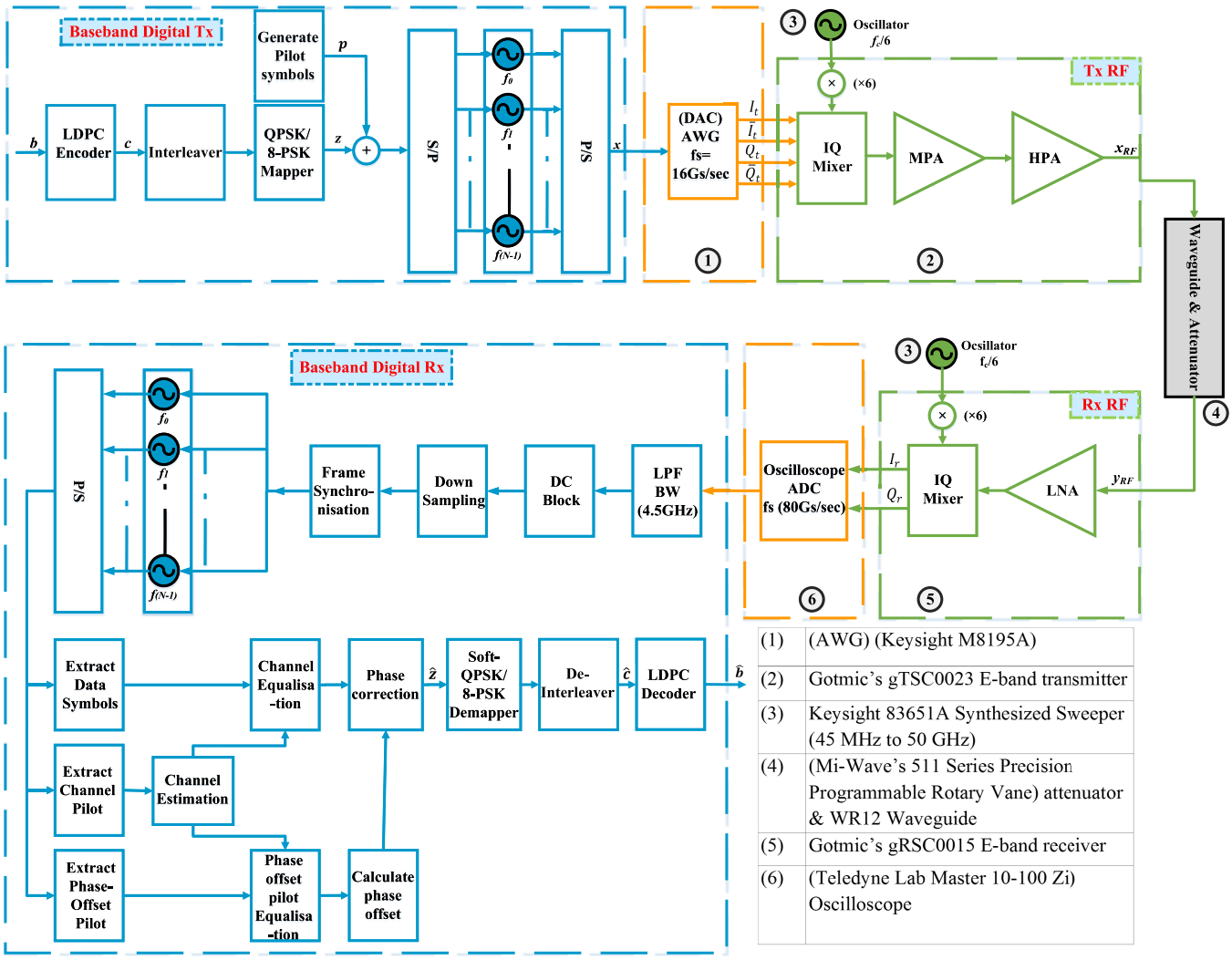

(1)	(AWG) (Keysight M8195A)
(2)	Gotmic's gTSC0023 E-band transmitter
(3)	Keysight 83651A Synthesized Sweeper (45 MHz to 50 GHz)
(4)	(Mi-Wave's 511 Series Precision Programmable Rotary Vane) attenuator & WR12 Waveguide
(5)	Gotmic's gRSC0015 E-band receiver
(6)	(Teledyne Lab Master 10-100 Zi) Oscilloscope

Fig. 6. Descriptive block diagram of the system with a list of the equipment used.

meaning that two parity bits are sent for each information bit. For more information about Shannon limit approaching FEC codes generally and LDPC specifically, readers are encouraged to read "Channel coding: The road to channel capacity" [44]. Furthermore, the implementation of LDPC codes with SEFDM has been investigated in [28] and the use of other coding techniques in [27] and [32].

The encoded bits $\mathbf{c} \in \{0, 1\}$ are interleaved by a block interleaver ($\prod$) of size 64,800 bits to scatter the burst errors. Hence, the possibility of loosing the information bit with its parity check bits reduces. The QPSK/8-PSK modulator maps each $\log_2(M)$ bits to a symbol z from the M-ary symbol alphabet, where $M = 4$ and $M = 8$ for the case of QPSK and 8-PSK, respectively. Thereafter, the mapped symbols' sequence $\mathbf{z}$ is divided into $N = 16$ parallel streams. Each symbol $z_{n^{\text{th}}}$ is modulated by the n^{th} subcarrier of the SEFDM symbol, where the frequency separation between adjacent subcarriers is ($\alpha \times BW/N = \alpha \times 250$ MHz). The spectrum of the resultant signal after RF upconversion is shown in Fig. 1.

In parallel to the process of preparing the message bits for SEFDM modulation, a pilot is generated. The pilot consists of five consecutive OFDM symbols, where the first pilot symbol is used to estimate the CFR coefficients and the other four are used to estimate the system phase offset. The pilot symbols have the same constellation order of the data symbols. The special feature of these pilot symbols is that they have the same frequency spacing ($\alpha \times 250$ MHz) and the number of subcarriers of SEFDM symbols, but they are orthogonal [31]. The orthogonality is maintained by increasing the pilot symbol duration T_p by a factor of $(1/\alpha)$, such as $T_p = T/\alpha$, and this implies that the pilot symbols are sent at a slower rate than that of the data symbols but occupy the same BW as SEFDM data symbols. For more details about this pilot structure, readers are referred to [31]. The added redundancy of this scheme depends on how frequent the pilot is sent. For instance, in this experiment, as the environment is static, the pilot is sent only once at the beginning before sending data of length $L_d = 3 \times 10^6$ symbols. Hence, the added redundancy, given by $((1-\alpha)/(L_d+1)) \times 100\%$ [31], is insignificant. Finally, the last stage is parallel to the serial converter, so the data stream generated is ready for the AWG IQ output.

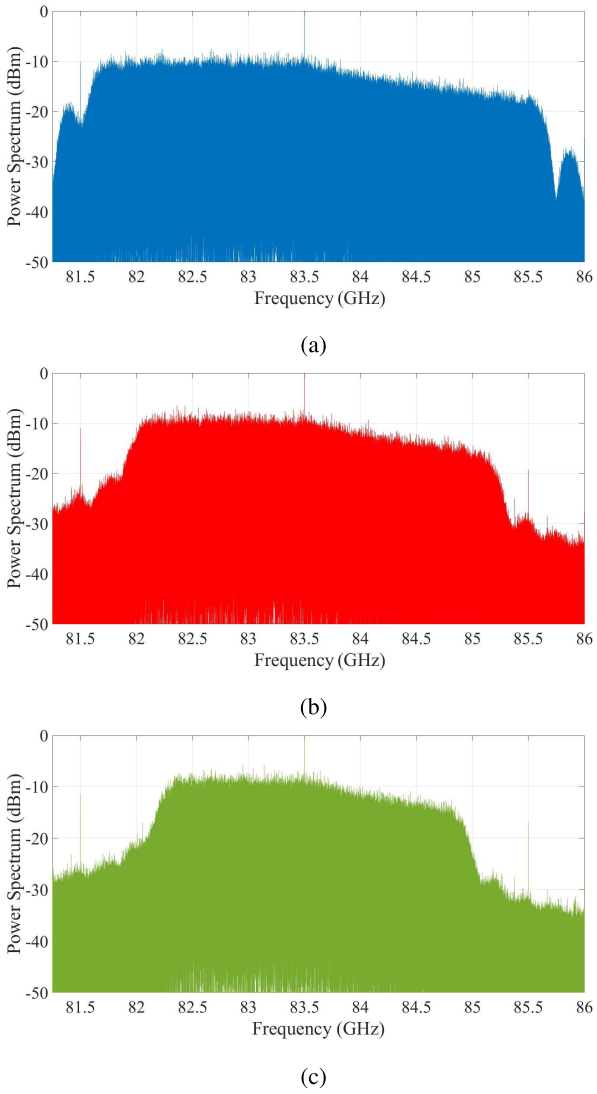

Fig. 7. Spectra of the received samples obtained from the experiment for OFDM ($\alpha = 1$) and SEFDM ($\alpha = 4/5$ and 2/3) for the same transmission rate 8 Gb/s. (a) OFDM ($\alpha = 1$), BW = 4 GHz. (b) SEFDM ($\alpha = 4/5$), BW = 3.2 GHz. (c) SEFDM ($\alpha = 2/3$), BW = 2.67 GHz.

Fig. 7 shows the spectrum of the received samples captured from the oscilloscope. It is important to note that the OOBE level of SEFDM is slightly lower than that of OFDM. For instance, the highest OOBE level is roughly -20 dBm for OFDM while it is lower than -20 and -22 dBm for SEFDM signals with $\alpha = 4/5$ and $\alpha = 2/3$, respectively. Consequently, extra subcarriers or signals of other users may use the saved BW. A digital low-pass filter of BW (4.5 GHz) is implemented followed by a dc block. Thereafter, a downsampler is used to resample the received data from 40 to 16 Gsample/s.

A new technique is developed in this paper for timing synchronization where the pilot symbols (used normally for the channel estimation) are also used here for timing synchronization. This is made possible due to the orthogonal nature of the pilot symbols, discussed above, allowing the known transmitted pilot samples to be correlated with the received samples at the receiver to give a correlation peak indicating

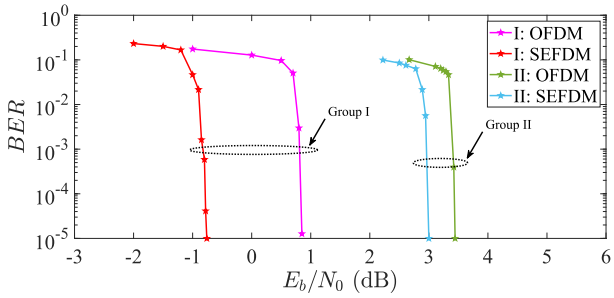

Fig. 8. Comparison of BER results versus E_b/N_0 for a given (α, $\log_2(M)$, R_c).

the beginning of the received data samples, thus establishing timing synchronization.

The received samples are demultiplexed into channel pilot symbol, phase offset pilot symbols, and data symbols. The channel pilot symbol enters the bank of demodulators; then, the output is used to estimate the CFR. Following, the phase offset pilot symbols are demodulated, then equalized using the estimated CFR and a one-tap equalizer. Afterward, the four equalized pilot symbols are used to calculate the phase offset. Here, four pilots are used for the phase offset estimation to gain a more accurate estimation. Thereafter, the received data symbols are equalized using a one-tap equalizer. Then, the equalized received symbols are rotated by the estimated phase offset. After this stage, the symbols are demapped, deinterleaved and decoded by an LDPC decoder with 50 iterations. The LDPC decoder uses what is called "message-passing algorithm," where the message is passed back and forward between the information bits and check nodes of the LDPC Tanner graph iteratively [44]. The output of the decoder is the estimated transmitted bits.

V. Measurement, Analysis, and Results

In this section, to evaluate the system performance and prove its viability, the analysis of the system setup and results are divided into four categories: simulation results; spectral efficiency gain; the advantage of OFDM pilot over SEFDM pilot; and SEFDM error performance.

A. Simulation Results

To begin with, the motivation behind SEFDM employment in this demonstration may be illustrated by considering Fig. 8. The error performance of baseband OFDM and SEFDM signals transmission over a flat AWGN channel is simulated using the digital baseband transmitter shown in Fig. 6 and the receiver in [28]. To allow fair comparison for given values of spectral efficiencies, both the bit rate and occupied BW were adjusted for SEFDM and OFDM. For clarity, the arrangement is held by subdividing the results into two groups according to the spectral efficiency (group I: 1 b/s/Hz; group II: 2.25 b/s/Hz). The spectral efficiency is varied by adjusting one of the three system parameters (α, $\log_2(M)$, R_c).

Looking at the BER curves of group I, OFDM (1, 2, 1/2) attains SEFDM (2/3, 2, 1/3) spectral efficiency by increasing

TABLE II

SPECTRAL EFFICIENCY AND CONSTELLATION OF THE EXPERIMENTALLY OBTAINED RECEIVED AND EQUALIZED SYMBOL BEFORE CHANNEL DECODING ON THE NINTH SUBCARRIER ($f = 83.5$ GHz) FOR DIFFERENT COMPRESSION FACTORS AND CONSTELLATION SIZES

M & R_b	Measurements	$\alpha = 1$	$\alpha = 4/5$	$\alpha = 2/3$
QPSK 8 Gbps	Constellation Before Equalization	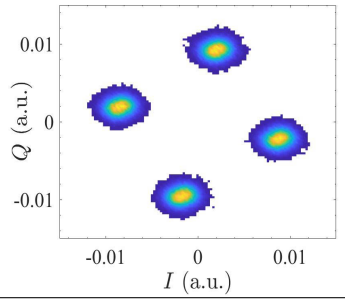	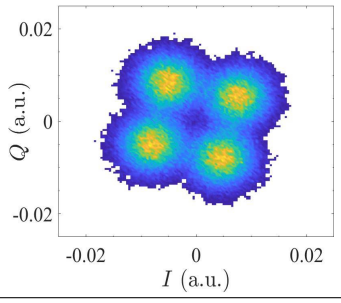	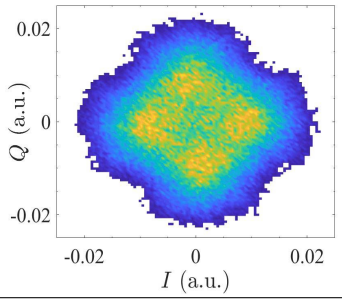
	Constellation After both Equalization and Phase Correction	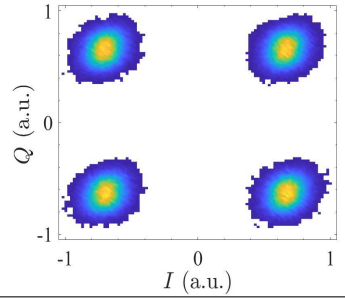	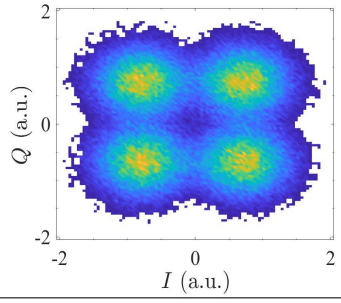	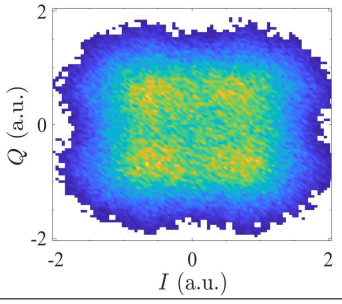
	Spectral Efficiency (η)	0.67 b/s/Hz	0.83 b/s/Hz	1 b/s/Hz
8PSK 12 Gbps	Constellation Before Equalization	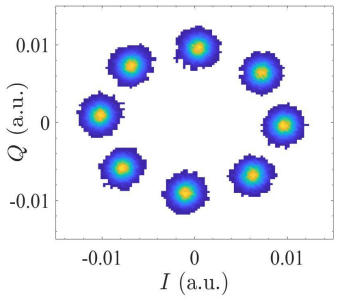	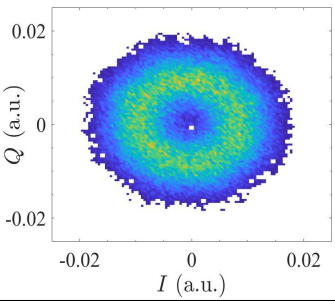	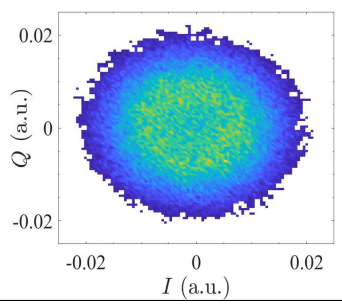
	Constellation After both Equalization and Phase Correction	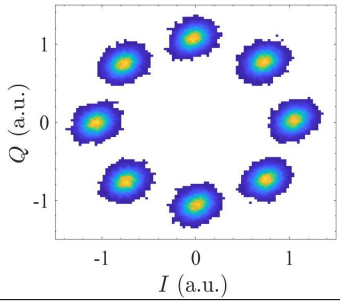	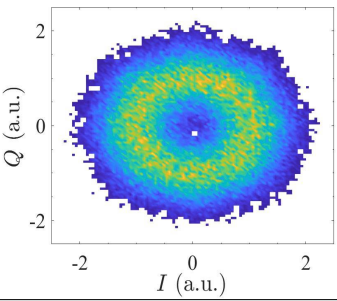	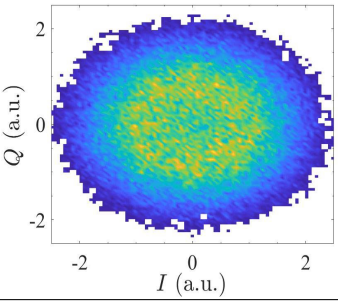
	Spectral Efficiency (η)	1 b/s/Hz	1.25 b/s/Hz	1.5 b/s/Hz

the coding rate. A 1.8 dB power savings may be achieved by compressing the BW rather than increasing the coding rate. The SEFDM power advantage reduces to 0.4 dB for higher modulation cardinality (8-PSK) as shown in group II, when SEFDM (4/5, 3, 3/5) is compared to OFDM (1, 3, 3/4). To conclude, at a given spectral efficiency, SEFDM saves BW compared to OFDM and requires less power while preserving the same BER performance.

B. SEFDM Spectral Efficiency Gain

The constellation diagrams of the received symbols, for QPSK and 8-PSK, before and after equalization and phase correction (before the decoder stage), are shown in Table II along with the spectral efficiency (η bit/s/Hz) for each case. This constellation is for the 9$^{\text{th}}$ subcarrier that is located at the center frequency ($f = 83.5$ GHz). It is chosen because compression is applied to its both sides; thus, this is the only subcarrier that has the same frequency for all the compression factors. Furthermore, the constellation given here is for the same Rx input power level, given the signal-to-noise ratio ($SNR = 25$ dB), where the transmission is error-free (i.e., BER $< 5 \times 10^{-6}$), even with the case of 8-PSK and $\alpha = 2/3$ due to the powerful LDPC decoder.

From Table II, we can notice that higher spectral efficiency improvement is gained for lower α and the percentile improvements (ζ), calculated by (6), are 25%, 50% for $\alpha = 4/5$ and $\alpha = 2/3$, respectively,

$$\zeta = \frac{\eta(\text{SEFDM}) - \eta(\text{OFDM})}{\eta(\text{OFDM})} \times 100\%. \tag{6}$$

This gain is achieved in this experiment as the transmitted SEFDM signal occupies less BW for the same OFDM signal transmission rate. Another scenario, which has not been tested yet but can be beneficial, is that of increasing the number of subcarriers for the SEFDM case to maintain OFDM BW rather than saving BW. For such case, the transmission data rate will be increased relative to OFDM.

C. SEFDM Versus OFDM Pilots

To evaluate the effect of the special OFDM pilot used to estimate the CFR and phase offset, a comparison is held when this pilot is used and when SEFDM pilots, similar to SEFDM transmitted data symbols, is used. The evaluation is done by checking the level of impairment on each transmitted symbol, using the root mean square (rms) of the normalized error vector magnitude (EVM) E_k of the data symbols after the equalization and phase offset correction stage at the same Rx input power value ($SNR = 25$ dB). The normalized EVM is calculated as

$$E_k = \sqrt{\frac{(I_k - \tilde{I}_k)^2 + (Q_k - \tilde{Q}_k)^2}{(I_k + Q_k)^2}}, \quad 1 \le k \le L_d \tag{7}$$

where L_d is the vector size of the transmitted symbols, I_k and Q_k are the in-phase and quadrature-phase elements of the k^{th} transmitted symbol, while $\tilde{I}_k$ and $\tilde{Q}_k$ are the in-phase and quadrature-phase elements of the k^{th} received symbol after equalization and phase correction. Consequently, the rms of EVM (EVM$_r$) is evaluated by taking the square root of the mean square of the EVM across all values. EVM$_r$ in decibel scale is given by

$$\text{EVM}_r = 20 \log \sqrt{\frac{1}{L_d} \sum_{k=1}^{L_d} {E_k}^2}. \tag{8}$$

Fig. 9 shows the advantage of using the special OFDM pilot over SEFDM pilot, where the EVM drops by approximately 2 and 2.5 dB for $\alpha = 4/5$ and $\alpha = 2/3$, respectively. The spectrum of the equalized received signal, obtained by the experiment, for the case of $\alpha = 0.8$, is shown for comparison. Clearly, the equalized spectrum using OFDM pilot is closer to ideal compared to that of the SEFDM pilot case.

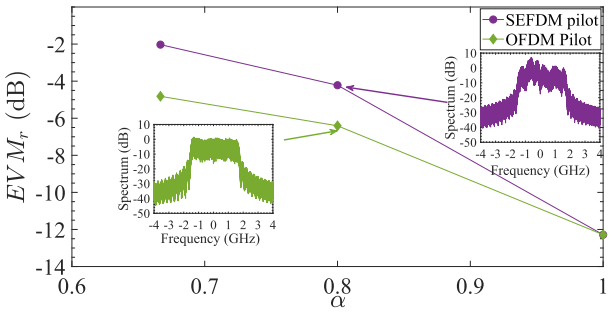

Fig. 9. EVM$_r$ calculation to compare the utilization of OFDM pilots over SEFDM pilots.

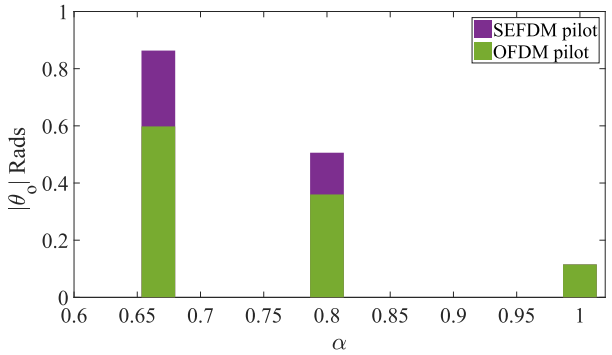

Fig. 10. Absolute phase difference calculation to compare the utilization of OFDM pilots over SEFDM pilots.

The advantage of such pilot design can also be considered from another perspective, by calculating the absolute phase difference between the transmitted and equalized symbols, using SEFDM and OFDM pilots. Fig. 10 demonstrates the absolute phase difference values for the OFDM and SEFDM pilots cases. From Fig. 10, it can be noticed that by using an OFDM pilot, the phase difference is lower compared to the case with SEFDM pilot. Furthermore, the phase difference increases by decreasing α (i.e., increase the compression level).

D. BER Results

Finally, due to the steep nature of the waterfall BER curves of LDPC coded schemes [44] and the measurement equipment limitations; specifically, the AWG buffer size limitation, the BER results collected lacked resolution and detail, and the error performance displayed either high numbers of errors or simply error-free behavior (i.e., $BER < 5 \times 10^{-6}$). As such, BER curves are not plotted here, instead Table III gives the Rx input SNR values for which the transmission becomes error-free, for different combinations of α and M used in the experiment, when (64 800$\times$90) bits are transmitted.

Clearly from Table III, the spectral efficiency improvement results in a power penalty of few decibels compared to OFDM.

TABLE III
MEASURED RX INPUT SNR VALUES FOR ERROR-FREE TRANSMISSION

M	α	SNR (dB)
4	1	5.1
4	4/5	6.5
4	2/3	8
8	1	7
8	4/5	9.2
8	2/3	11.8

For instance, for the QPSK case, 1.4 and 2.9 dB increase in the power level is required, to increase the spectral efficiency by 25% and 50%, respectively. On the other hand, for the higher constellation order (8-PSK), the signal appears to be slightly more sensitive to BW compression, resulting in a slightly higher power penalty. It is worth noting that the noise level and nonlinear impairments of the time-interleaved high-speed oscilloscope scale with the power of the received signal; therefore, in a more ideal setup, the *SNR* required to achieve the error-free operation may be lower (better) than what is measured and reported here in Table III.

Previous work has shown that this penalty gap can be further reduced, by using a more sophisticated receiver design, which estimates the interference and cancels it gradually in an iterative manner [28], [32]. However, as the aim of this demonstration is to validate the concept of utilizing SEFDM for the E-band data transmission, a simple detector similar to OFDM is used, which can be implemented in real time.

Finally, referring to Table III and the reported attenuation levels from the digital attenuator (item 4 shown in Fig. 6) for each SNR value, coupled with a 46 dBi gain E-band antenna at both the Tx and Rx, it can be anticipated that the best-case hop link is between 2.4 and 4.1 km. Such calculation takes into account the free space path loss only, without other impairments like oxygen absorption, rain, humidity, and others. Thus, they are the upper bound distance values for future experiments, where the E-band link will be affected by environmental and weather conditions.

VI. CONCLUSION

This paper reports, for the first time, the application of the special multicarrier signaling format SEFDM in an E-band (81–86 GHz) millimeter-wave system. SEFDM has the advantage of offering substantial spectral efficiency advantages by saving BW in wireless and wired communication systems, and this paper verifies such advantages experimentally and through the design and testing of multi-gigabits per second communication link operating in the 81–86 GHz frequency region.

The presented experimental demonstration of SEFDM transmission utilizes GaAs microwave integrated circuits transceiver chips, for conversion from baseband to RF spectrum and vice versa. The suitability of such circuits was evaluated and proven in a specially designed test bed. The overall system CFR has been estimated using a newly developed channel estimation scheme for SEFDM. This estimation scheme showed Tx–Rx EVM measurements' enhancement by up to 2.5 dB, when compared to conventional channel estimation schemes. The combination of this estimation scheme and the powerful LDPC channel coding achieves the highest transmission rate of 12 Gb/s. Such transmission rate is demonstrated over BWs ranging from 4 GHz for a noncompressed system down to 2.67 GHz for an SEFDM system.

This paper demonstrates that in the E-band, the use of multicarrier transmission, with judicious selection of modulation format and SEFDM signal compression, allows up to 50% improvement in spectral efficiency (relative to OFDM or single-carrier uncompressed systems) with some loss of performance that may be ameliorated by using more sophisticated detection techniques.

ACKNOWLEDGMENT

The authors would like to thank G. Granström from Gotmic AB, Gothenburg, Sweden, for his assistance with the characterization of the transmitter and the receiver.

REFERENCES

[1] P. Wang, Y. Li, L. Song, and B. Vucetic, "Multi-gigabit millimeter wave wireless communications for 5G: From fixed access to cellular networks," *IEEE Commun. Mag.*, vol. 53, no. 1, pp. 168–178, Jan. 2015.

[2] Y. Shoji, C. S. Choi, and H. Ogawa, "70-GHz-Band OFDM transceivers based on self-heterodyne Scheme for millimeter-wave wireless personal area network," *IEEE Trans. Microw. Theory Techn.*, vol. 54, no. 10, pp. 3664–3674, Oct. 2006.

[3] T. Rappaport, R. Heath, R. Daniels, and J. Murdock, *Millimeter Wave Wireless Communications*. Upper Saddle River, NJ, USA: Prentice-Hall, 2015.

[4] C. S. Choi, Y. Shoji, and H. Ogawa, "Implementation of an OFDM baseband with adaptive modulations to grouped subcarriers for millimeter-wave wireless indoor networks," *IEEE Trans. Consum. Electron.*, vol. 57, no. 4, pp. 1541–1549, Nov. 2011.

[5] C. Y. Lin, Y. C. Chi, C. T. Tsai, H. Y. Wang, and G. R. Lin, "39-GHz millimeter-wave carrier generation in dual-mode colorless laser diode for OFDM-MMWoF transmission," *IEEE J. Sel. Topics Quantum Electron.*, vol. 21, no. 6, pp. 609–618, Nov. 2015.

[6] Z. Cao *et al.*, "61.3-Gbps hybrid fiber-wireless in-home network enabled by optical heterodyne and polarization multiplexing," *J. Lightw. Technol.*, vol. 32, no. 19, pp. 3227–3233, Oct. 1, 2014.

[7] M. T. Martinez-Ingles, C. Sanchis-Borras, J. M. Molina-Garcia-Pardo, J. V. Rodriguez, L. Juan-Llácer, "Experimental evaluation of an indoor MIMO-OFDM system at 60 GHz based on the IEEE802.15.3c standard," *IEEE Antennas Wireless Propag. Lett.*, vol. 12, pp. 1562–1565, Nov. 2013.

[8] C. Sanchis-Borrás, M. T. Martínez-Inglés, J. M. Molina-García-Pardo, J. P. García, and J. V. Rodriguez, "Experimental study of MIMO-OFDM transmissions at 94 GHz in indoor environments," *IEEE Access*, vol. 5, pp. 7488–7494, Apr. 2017.

[9] S. Nie, G. R. MacCartney, S. Sun, and T. S. Rappaport, "72 GHz millimeter wave indoor measurements for wireless and backhaul communications," in *Proc. IEEE 24th Annu. Int. Symp. PIMRC*, Sep. 2013, pp. 2429–2433.

[10] G. R. MacCartney and T. S. Rappaport, "73 GHz millimeter wave propagation measurements for outdoor urban mobile and backhaul communications in New York City," in *Proc. IEEE ICC*, Jun. 2014, pp. 4862–4867.

[11] V. Dyadyuk *et al.*, "A Multigigabit millimeter-wave communication system with improved spectral efficiency," *IEEE Trans. Microw. Theory Techn.*, vol. 55, no. 12, pp. 2813–2821, Dec. 2007.

[12] X. Zhang, L. Chen, J. Qiu, and J. Abdoli, "On the waveform for 5G," *IEEE Commun. Mag.*, vol. 54, no. 11, pp. 74–80, Nov. 2016.

[13] L. Zhang, A. Ijaz, P. Xiao, M. M. Xiao, and R. Tafazolli, "Filtered OFDM systems, algorithms, and performance analysis for 5G and Beyond," *IEEE Trans. Commun.*, vol. 66, no. 3, pp. 1205–1218, Mar. 2018.

[14] C. Kim, Y. H. Yun, K. Kim, and J. Y. Seol, "Introduction to QAM-FBMC: From waveform optimization to system design," *IEEE Commun. Mag.*, vol. 54, no. 11, pp. 66–73, Nov. 2016.

[15] J. E. Mazo, "Faster-than-nyquist signaling," *Bell Syst. Tech. J.*, vol. 54, no. 8, pp. 1451–1462, Oct. 1975.

[16] M. Rodrigues and I. Darwazeh, "A spectrally efficient frequency division multiplexing based communications system," in *Proc. 8th Int. OFDM Workshop*, Hamburg, Germany, Nov. 2003, pp. 48–49.

[17] F. Rusek and J. B. Anderson, "Multistream faster than nyquist signaling," *IEEE Trans. Commun.*, vol. 57, no. 5, pp. 1329–1340, May 2009.

[18] J. B. Anderson, F. Rusek, and V. öwall, "Faster-than-Nyquist signaling," *Proc. IEEE*, vol. 101, no. 8, pp. 1817–1830, Aug. 2013.

[19] J. Zhou *et al.* "Capacity limit for faster-than-Nyquist non-orthogonal frequency-division multiplexing signaling," *Sci. Rep.*, vol. 7, p. 3380, Jun. 2017.

[20] M. R. Khanzadi, D. Kuylenstierna, A. Panahi, T. Eriksson, and H. Zirath, "Calculation of the performance of communication systems from measured oscillator phase noise," *IEEE Trans. Circuits Syst. I, Reg. Papers*, vol. 61, no. 5, pp. 1553–1565, May 2014.

[21] J. Chen *et al.*, "Does LO noise floor limit performance in multi-gigabit millimeter-wave communication?" *IEEE Microw. Wireless Compon. Lett.*, vol. 27, no. 8, pp. 769–771, Aug. 2017.

[22] J. Chen *et al.*, "Influence of white LO noise on Wideband communication," *IEEE Trans. Microw. Theory Techn.*, vol. 66, no. 7, pp. 3349–3359, Jul. 2018.

[23] I. Kanaras, A. Chorti, M. R. D. Rodrigues, and I. Darwazeh, "A fast constrained sphere decoder for Ill conditioned communication systems," *IEEE Commun. Lett.*, vol. 14, no. 11, pp. 999–1001, Nov. 2010.

[24] T. Xu, R. C. Grammenos, F. Marvasti, and I. Darwazeh, "An improved fixed sphere decoder employing soft decision for the detection of non-orthogonal signals," *IEEE Commun. Lett.*, vol. 17, no. 10, pp. 1964–1967, Oct. 2013.

[25] S. V. Zavjalov, S. V. Volvenko, and S. B. Makarov, "A method for increasing the spectral and energy efficiency SEFDM signals," *IEEE Commun. Lett.*, vol. 20, no. 12, pp. 2382–2385, Dec. 2016.

[26] M. Jia, Z. Yin, Q. Guo, G. Liu, and X. Gu, "Downlink design for spectrum efficient IoT network," *IEEE Internet Things J.*, vol. 5, no. 5, pp. 3397–3404, Oct. 2018.

[27] H. Ghannam and I. Darwazeh, "Signal coding and interference cancellation of spectrally efficient FDM systems for 5G cellular networks," in *Proc. 24th ICT*, May 2017, pp. 1–6.

[28] H. Ghannam and I. Darwazeh, "SEFDM over satellite systems with advanced interference cancellation," *IET Commun.*, vol. 12, no. 1, pp. 59–66, Jan. 2018.

[29] S. Isam and I. Darwazeh, "Robust channel estimation for spectrally efficient FDM system," in *Proc. 19th ICT*, Apr. 2012, pp. 1–6.

[30] Y. Wang *et al.*, "Efficient MMSE-SQRD-based MIMO decoder for SEFDM-based 2.4-Gb/s-spectrum-compressed WDM VLC system," *IEEE Photon. J.*, vol. 8, no. 4, pp. 1–9, Aug. 2016.

[31] H. Ghannam and I. Darwazeh, "Robust channel estimation methods for spectrally efficient FDM systems," in *Proc. IEEE 87th Veh. Technol. Conf. (VTC)*, Jun. 2018, pp. 1–6.

[32] T. Xu, S. Mikroulis, J. E. Mitchell, and I. Darwazeh, "Bandwidth compressed waveform for 60-GHz millimeter-wave radio over fiber experiment," *J. Lightw. Technol.*, vol. 34, no. 14, pp. 3458–3465, Jul. 15, 2016.

[33] T. Xu and I. Darwazeh, "Transmission experiment of bandwidth compressed carrier aggregation in a realistic fading channel," *IEEE Trans. Veh. Technol.*, vol. 66, no. 5, pp. 4087–4097, May 2017.

[34] I. Darwazeh, T. Xu, T. Gui, Y. Bao, and Z. Li, "Optical SEFDM system; bandwidth saving using non-orthogonal sub-carriers," *IEEE Photon. Technol. Lett.*, vol. 26, no. 4, pp. 352–355, Feb. 15, 2014.

[35] D. Nopchinda, T. Xu, R. Maher, B. C. Thomsen, and I. Darwazeh, "Dual polarization coherent optical spectrally efficient frequency division multiplexing," *IEEE Photon. Technol. Lett.*, vol. 28, no. 1, pp. 83–86, Jan. 1, 2016.

[36] T. Xu and I. Darwazeh, "Experimental validations of bandwidth compressed multicarrier signals," in *Proc. IEEE 17th Int. Symp. WoWMoM*, Jun. 2016, pp. 1–10.

[37] I. Darwazeh, H. Ghannam, and T. Xu, "The first 15 years of SEFDM: A brief survey," in *Proc. 11th Int. Symp. CSNDSP*, Jul. 2018, pp. 1–7.

[38] R. Gallager, "Low-density parity-check codes," *IRE Trans. Inf. Theory*, vol. 8, no. 1, pp. 21–28, Jan. 1962.

[39] *3rd Generation Partnership Project; Technical Specification Group Radio Access Network; Study on New Radio (NR) Access Technology (Release 14)*, document TR 38.912 version 14.0.0, 3GPP, Jun. 2017.

[40] S. Isam and I. Darwazeh, "Characterizing the intercarrier interference of non-orthogonal spectrally efficient FDM system," in *Proc. 8th Int. Symp. CSNDSP*, Jul. 2012, pp. 1–5.

[41] *Gotmic*. Accessed: Jan. 10, 2018. [Online]. Available: http://www.gotmic.se

[42] M. Gavell, H. Zirath, M. Ferndahl, and S. E. Gunnarsson, "A linear 70-95 GHz differential IQ modulator for E-band wireless communication," in *IEEE MTT-S Int. Microw. Symp. Dig.*, May 2010, pp. 788–791.

[43] D. Nopchinda, Z. He, G. Granström, M. Gavell, and H. Zirath, "8-PSK Upconverting transmitter using E-band frequency sextupler," *IEEE Microw. Wireless Compon. Lett.*, vol. 28, no. 2, pp. 177–179, Feb. 2018.

[44] D. J. Costello and G. D. Forney, "Channel coding: The road to channel capacity," *Proc. IEEE*, vol. 95, no. 6, pp. 1150–1177, Jun. 2007.

Hedaia Ghannam (S'13) received the B.Sc. degree (Hons.) in electrical engineering from the Princess Sumaya University for Technology, Amman, Jordan, in 2011, and the M.Sc. degree (Hons.) in telecommunication and information systems from the University of Essex, Colchester, U.K., in 2014. She is currently pursuing the Ph.D. degree at the Communication and Information System Research Group, Department of Electronics and Electrical Engineering, University College London, London, U.K.

Her current research interests include the physical layer of future communication systems, such as the fifth-generation cellular network and E-band transmission systems, where she looks at the system from different aspects including spectrally efficient modulation formats, channel coding, and the design of practical channel estimators and detectors for the aforementioned systems.

Ms. Ghannam was a recipient of the Overseas Research Student Award and the Dean Prize to study at University College London, HESPAL Scholarship for her M.Sc. research. She was the recipient of the Turing Institute Prize in 2017 and the EPSRC Impact Acceleration Account Funding in 2018. She was also the recipient of the Best Project Award.

Dhecha Nopchinda (S'12) was born in Bangkok, Thailand, in 1991. He received the B.Eng. degree (Hons.) in electronics and communication engineering from the Sirindhorn International Institute of Technology, Thammasat University, Bangkok, in 2013, the M.Sc. degree (Hons.) in wireless and optical communications from University College London, London, U.K., in 2014, and the Lic.Eng. degree from the Chalmers University of Technology, Gothenburg, Sweden, in 2017, where he is currently pursuing the Ph.D. degree at the Microwave Electronics Laboratory under the main supervision of Prof. H. Zirath.

His current research interests include digital techniques for high data-rate communication and microwave measurements at millimeter wave.

Mr. Nopchinda was a recipient of a scholarship to study at the Sirindhorn International Institute of Technology.

Marcus Gavell (GS'09) was born in Eskilstuna, Sweden, in 1981. He received the M.Sc. and Ph.D. degrees in electrical engineering from the Chalmers University of Technology, Gothenburg, Sweden, in 2005 and 2018, respectively.

In 2008, he joined Gotmic AB, Gothenburg, after working as a Radio Verification Engineer with Ericsson AB. Since 2015, he has been the CTO with Gotmic AB. His current research interests include millimeter-wave MMIC design, in particular, transmitters, receivers, power amplifiers, and predistortion circuits.

Herbert Zirath (M'86–SM'08–F'11) was born in Gothenburg, Sweden, in 1955. He received the M.Sc. and Ph.D. degrees in electrical engineering from the Chalmers University of Technology, Gothenburg, in 1980 and 1986, respectively.

From 1986 to 1996, he was a Researcher with the Department of Radio and Space Science, Chalmers University of Technology, where he was responsible for developing GaAs- and InP-based HEMT technology, including devices, models, and circuits. In 1998, he joined the California Institute of Technology, Pasadena, CA, USA, as a Research Fellow, where he was engaged in the design of monolithic microwave integrated circuit (MMIC) frequency multipliers and class-E power amplifiers. In 2001, he joined the Chalmers University of Technology, as the Head of the Microwave Electronics Laboratory, where he has been a Professor of high speed electronics with the Department of Microtechnology and Nanoscience since 1996. He is currently leading a group of approximately 40 researchers in the area of high-frequency semiconductor devices and circuits. He is a Research Fellow with Ericsson AB, leading the development of a D-band (110–170-GHz) chipset for high data-rate wireless communication. He is a co-founder of Gotmic AB, Gothenburg, a company developing highly integrated front-end MMIC chip sets for 60 GHz and E-band wireless communication. He has authored or co-authored over 600 refereed journals/conference papers and has an H-index of 43 and holds 5 patents. His current research interests include MMIC designs for wireless communication and sensor applications based on III–V, III–N, graphene, and silicon devices.

Izzat Darwazeh (SM'03) received the bachelor's degree in electrical engineering from The University of Jordan, Amman, Jordan, in 1984, and the M.Sc. and Ph.D. degrees from The University of Manchester, Manchester, U.K., in 1986 and 1991, respectively.

In 2002, he proposed (with M. Rodrigues) the fast OFDM concept and, in 2003, the SEFDM concept, and has been focusing on these topics since that time. He is currently the University of London Chair of Communications Engineering. He leads the 70 Strong Communications and Information Systems Group, Department of Electronic and Electrical Engineering, University College London (UCL), London, U.K, where he is also the Director of ICCS, UCL Institute of Communications and Connected Systems. He teaches mobile and wireless communications and circuit design. He has authored or co-authored over 250 papers and book chapters in the areas of optical and wireless communications and monolithic microwave integrated circuits and high-speed/frequency circuits. He was a Co-Editor of the *Analogue Optical Fibre Communications* (IEE, 1995) and a 2008 Elsevier–Newness book on electrical engineering. He co-authored *Linear Circuit Analysis and Modelling* (Elsevier, 2005) and *Microwave Active Circuit Analysis and Design* (Academic, 2015). His current research interests include ultrahigh-speed microwave circuits and wireless and optical communication systems.

Dr. Darwazeh is a Chartered Engineer in the U.K. He is a Fellow of the IET and the Institute of Telecommunications Professionals.